



Dynamical processes controlling the evolution of early-summer cut-off lows in Northeast Asia

Yu Nie^{1,3} · Yang Zhang² · Jinqing Zuo¹ · Mengling Wang² · Jie Wu¹ · Ying Liu¹

Received: 29 December 2021 / Accepted: 27 May 2022 / Published online: 20 June 2022
© The Author(s) 2022

Abstract

Cut-off lows are crucial extratropical circulation systems that can bring weather extremes over large areas, but the mechanism responsible for the life cycle of cut-off lows remains elusive. From a perspective of regional eddy-mean flow interaction, this study investigates the dynamical processes controlling the evolution of early-summer cut-off lows over Northeast Asia using the 6-hourly reanalysis data. Through the diagnostic of local wave activity (LWA) budget, we show that the cut-off low is initialized by a Rossby wave train originated from the subpolar North Atlantic, and then reinforced rapidly by zonal LWA flux convergence and local baroclinic eddy generation, and eventually decayed through energy dispersion by zonal wave activity advection. Furthermore, we show that the evolutions of the above dynamical processes are strongly modulated by the changes of background flow. In early summer, Northeast Asia is located at the eastern exit of the midlatitude jet to the north of the subtropical jet and exhibits a weak meridional gradient of potential vorticity, which favors frequent formation of cyclonic anomaly and energy accumulation. Prior to the onset of cut-off lows by several days, a Rossby wave train propagates along the Eurasian midlatitude jet, which initializes a cyclonic anomaly over Northeast Asia. With the aid of mean flow advection of anomalous zonal momentum, the zonal winds are then decelerated at the midlatitude jet exit and accelerated at the subtropical jet center. The former obstructs the wave packet proceeding downstream and the latter favors stronger baroclinic eddy generation below the subtropical jet. The two processes together maintain and strengthen the cyclonic anomaly in Northeast Asia rapidly.

Keywords Cut-off lows · Regional eddy-mean flow interaction · Finite-amplitude wave activity · Northeast Asia

1 Introduction

Cut-off lows are enclosed cyclonic circulations equatorward of the deep troughs above cold surface anomalies (Palmen and Newton 1969), which can often bring moderate to heavy rainfall (He et al. 2006; Wang et al. 2007; Hu et al. 2011) and persistent cool weather (Gao et al. 2014; Xie and Bueh

2015) over large areas. In particular, they are among the most important circulation systems that are responsible for some of the most catastrophic flood (Zhao and Sun 2007). Multiple studies have suggested that Northeast Asia is one of the most preferred regions for frequent occurrences of cut-off lows in the Northern Hemisphere (e.g., Nieto et al. 2005). The Northeast Asian cut-off lows are statistically most common in early summer, particularly in May and June (Yang et al. 2021).

Since cut-off lows over Northeast Asia have severe impacts on regional extremes, a lot of progress has been made to understand their large-scale circulation features and external forcings on seasonal and longer time scales. In mid-to-high latitudes, strong blocking highs over Ural mountain and Ochotsk sea are often observed in the upstream and downstream sides of cut-off lows (Hu et al. 2011). Meandering of prevailing westerly jet streams is also closely related to cut-off lows. A split-jet structure in the upstream is favorable for frequent occurrence of cut-off lows, and persistent cyclonic reversal of the East Asian jet can cause a cut-off low in a prolonged period. In subtropics, the western Pacific high is

✉ Yang Zhang
yangzhang@nju.edu.cn

¹ Laboratory for Climate Studies, CMA-NJU Joint Laboratory for Climate Prediction Studies, National Climate Center, China Meteorological Administration, Beijing, China
² CMA-NJU Joint Laboratory for Climate Prediction Studies, Institute for Climate and Global Change Research, School of Atmospheric Sciences, Nanjing University, Nanjing, China
³ Collaborative Innovation Center on Forecast and Evaluation of Meteorological Disasters (CIC-FEMD), Nanjing University of Information Science & Technology, Nanjing, China

stronger when the cut-off low occurs (Xie and Bueh 2015). Given these understandings on circulation features, Wang et al. (2018) further showed that the summertime cut-off lows are also driven by external thermal forcing, including the cold anomalies of offshore sea surface temperature, and cold anomalies of land surface temperature over west Asia in the preceding spring. Using an idealized linear baroclinic model, Lin and Bueh (2021) refreshes the understanding of the topic by emphasizing the important role of the diabatic heating in forcing the summertime East Asian low.

On the subseasonal time scale, observational studies have shown that the summertime cut-off lows over Northeast Asia exhibit strong variability in strength. Lin and Bueh (2021) attributed the weaker intensity of the cut-off lows in August to the enhanced offset effect of radiative cooling. By analyzing typical cases of cut-off lows, Lian et al. (2010) showed that strong cut-off lows are often accompanied by persistent Ural blocking highs that are mainly maintained through Rossby wave dispersion and transient eddy forcing. Using daily reanalysis data, Liu et al. (2012) further showed that the low-frequency variation of the cut-off low is associated with a convergence between the Eurasian (EU) teleconnection pattern and East Asian-Pacific (EAP) pattern. Xie and Bueh (2015) further classified cut-off lows into four typical types based on the location of ridges close to the cut-off low and investigated their different impacts on cold surface air temperatures. These understandings on the circulation features of the cut-off low variabilities indicate that low-frequency Rossby wave train, upstream blocking high as well as the local diabatic heating may play a role in the formation of Northeast Asian cut-off lows. However, the relative contribution of these different processes in the evolution of cut-off lows remains not clearly quantified (Lian et al. 2016).

Recent studies by Huang and Nakamura (2015) and Nakamura and Huang (2018) introduced a local finite amplitude wave activity (LWA) budget analysis, which proves to be very efficient in quantifying the local eddy-mean flow interaction in the analysis of blocking high evolution. In a recent development of the formalism, contributions of upstream wave train, local baroclinic eddy generation as well as diabatic heating can be explicitly diagnosed (Wang et al. 2021). With a focus on the subseasonal time scale, this study will apply this newly developed LWA budget analysis to quantify the Rossby wave train, local transient eddy forcing, and diabatic heating in the life cycle of early-summer cut-off lows over Northeast Asia. We show that an initial Rossby wave train from the subpolar North Atlantic helps to form a cyclonic anomaly in Northeast Asia. Then the cyclonic anomaly is amplified rapidly through both zonal LWA flux convergence from the upstream and local baroclinic eddy generation. We further argue that these dynamical processes are strongly modulated by the background zonal wind, meridional potential vorticity gradient and temperature gradient. The paper

is organized as follows. In Sect. 2, we describe the data and diagnostic methods. The dynamical evolution of cut-off lows is diagnosed through LWA budget in Sect. 3. Modulation of background flow on the dynamical processes are discussed in Sect. 4. Section 5 summarizes our results.

2 Data and methods

2.1 Reanalysis data

We use zonal wind, meridional wind, air temperature and geopotential height from the fifth generation of atmospheric reanalysis in European Centre for Medium-Range Weather Forecasts (ERA5 reanalysis) (Hersbach et al. 2020). The data analyzed are 6-hourly on the $1^\circ \times 1^\circ$ longitude-latitude grids for the period of 1979–2020. The diabatic heating output at the same resolution from the Climate Forecast System Reanalysis (CFSR) dataset during 1979–2010 is also employed to test the robustness of our results (Saha et al. 2014). Only the early-summer (May and June) fields are analyzed in this paper.

2.2 Cut-off low detection via Local wave activity

Commonly, blocking highs and cut-off lows are measured empirically by the wave amplitude (Screen and Simmonds 2013), sinuosity (Cattiaux et al. 2016), or meridional reversal (Tibaldi and Molteni 1990) of mid-tropospheric geopotential height, but the weather events detected by each method may vary considerably, as different methods highlight different features of blocking/cut-off events. In this study, the cut-off low is objectively diagnosed by a local wave activity (LWA) based on the geopotential height at 500 hPa (LWA_{Z500}) as in Chen et al. (2015), which has been widely used in multiple analyses of blocking and wave events (Martineau et al. 2017; Ghinassi et al. 2018; Chen et al. 2022). The LWA_{Z500} dynamically measures the waviness of the mid-tropospheric geopotential height contour and yields a daily two-dimensional (longitude-latitude) map. Specifically, the LWA of geopotential height at longitude λ and latitude ϕ_e is defined as:

$$LWA_{Z500}(\lambda, \phi_e) = \underbrace{\frac{a}{\cos \phi} \int_{z_e \geq 0, \phi \geq \phi_e} z_e(\lambda, \phi) \cos \phi d\phi}_{\text{anticyclonic}} - \underbrace{\frac{a}{\cos \phi} \int_{z_e \leq 0, \phi \leq \phi_e} z_e(\lambda, \phi) \cos \phi d\phi}_{\text{cyclonic}}. \quad (1)$$

Here ϕ_e is the equivalent latitude of the geopotential height contour at 500 hPa. $z_e(\lambda, \phi) = z(\lambda, \phi) - Z_{500}(\phi_e)$ is an eddy term describing the deviation of the geopotential height

contour from the eddy-free, zonally symmetric basic state. More details on the $LWA_{Z_{500}}$ can be referred to Chen et al. (2015).

To analyze the time evolution of cut-off lows, we define a daily cut-off low index as the normalized time series of domain-averaged cyclonic component of $LWA_{Z_{500}}$ over Northeast Asia (35° – 55° N, 115° – 145° E). The key region is consistent with multiple previous studies on cold vortex over Northeast Asia (Hu et al. 2010, 2011; Xie and Bueh 2015). The linear long-term trend of the index is removed here to eliminate its impact on subseasonal variability of cut-off lows. By construction, positive values of the index correspond to stronger-than-normal cut-off lows in Northeast Asia. The circulation and eddy characteristics associated with cut-off lows are investigated through lagged composites of these fields for the positive phase of cut-off low index (larger than its time mean by one standard deviation). Figure 1 shows the composite maps of Z_{500} and $LWA_{Z_{500}}$ anomalies at the peak dates of strong cut-off lows. The total Z_{500} (black contours) shows a strong trough in Northeast Asia, with an enclosed contour in the trough center (Fig. 1a), demonstrating that the cut-off low index based on $LWA_{Z_{500}}$

can well capture the typical characteristics of cut-off lows. The Z_{500} anomalies (shading) exhibit strong negative values in the trough center and relatively weak positive values to the northwest of the trough. The $LWA_{Z_{500}}$ in Fig. 1b shows strong positive anomalies over Northeast Asia, suggesting that the cut-off low is often accompanied with a strong wave activity anomaly. The lower panel of Fig. 1 shows the composite maps of q_{250} and $LWA_{q_{250}}$ anomalies at peak days. Both composite maps of q_{250} and $LWA_{q_{250}}$ display strong positive anomalies in the cut-off low region, which is consistent with the strong positive anomalies of $LWA_{Z_{500}}$ shown in Fig. 1b. The q_{250} and $LWA_{q_{250}}$ also display negative anomalies in the southeastern area, which is due to the vertical structure of midlatitude waves. Since many previous studies on blockings and cut-off lows are based on the waviness or meridional reversal of Z_{500} , we choose to use the $LWA_{Z_{500}}$ to define the cut-off low index to be consistent with those works. Note that the results in this study are not sensitive to the choice of domain and index definition method (Fig. S1), although the intensity of Z_{500} anomalies is stronger because we select those cut-off lows stronger than one standard deviation of the $LWA_{Z_{500}}$ index.

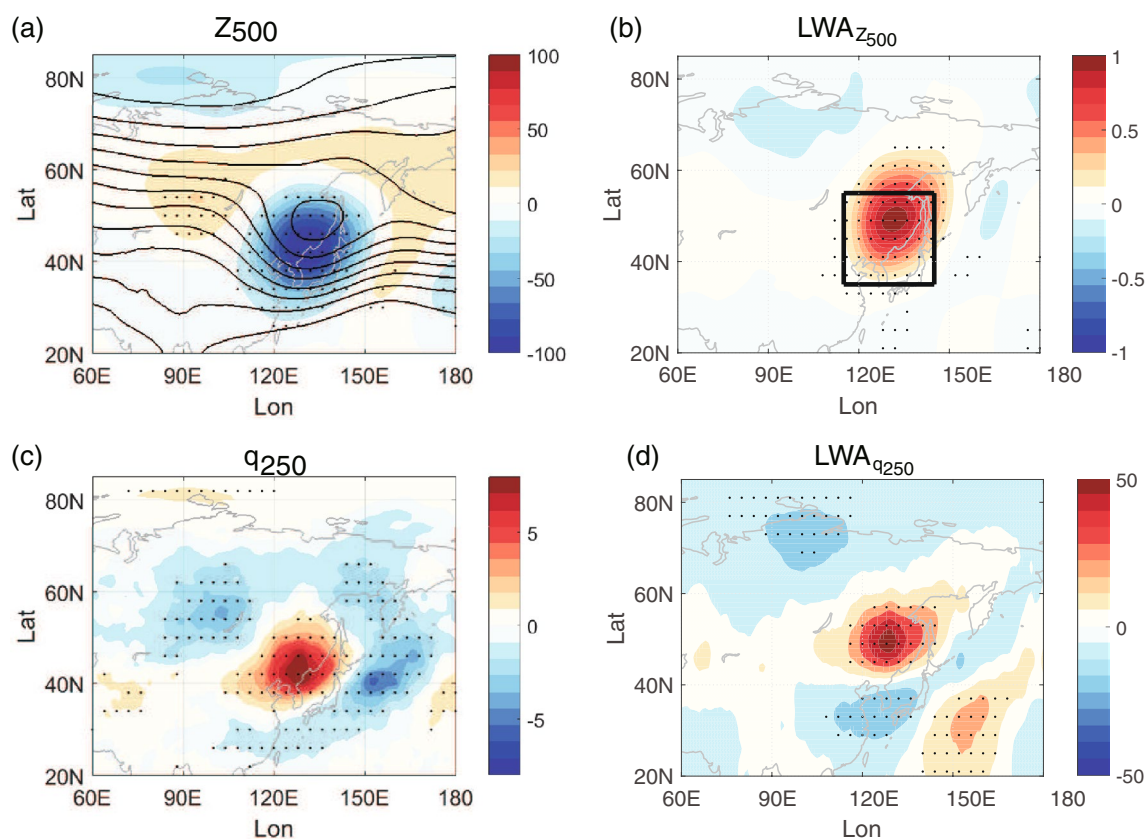


Fig. 1 Composite maps of the **a** total Z_{500} (black contours with interval of 50 m) and Z_{500} anomaly (shading, unit: m), **b** $LWA_{Z_{500}}$ anomaly (10^8 m^2), **c** q_{250} anomaly (day^{-1}) and **d** $LWA_{q_{250}}$ anomaly (ms^{-1}) for strong cut-off lows at lag 0 day over Northeast Asia in early summer.

The black box in **(b)** denotes the key region of the Northeast Asian cut-off lows (115° – 145° E, 35° – 55° N). Values that are significant at the 95% confidence level are highlighted with black dots

2.3 Local wave activity budget

To analyze the dynamical processes responsible for the evolution of cut-off lows, we have also employed the LWA budget developed by Huang and Nakamura (2015) and Wang et al. (2021) based on the potential vorticity at 250 hPa (LWA_{q250}). The 250-hPa LWA is used here because primary contributions to the column LWA come from the upper troposphere (Huang and Nakamura 2015, 2017) and the horizontal wave propagation is strongest in the upper troposphere.

The quasi-geostrophic PV is computed as $q = f + \zeta + f \frac{\partial}{\partial p} \left[\frac{\theta - \theta_0}{\partial \theta_0 / \partial p} \right]$, where f and ζ denote the planetary vorticity and relative vorticity respectively. θ_0 is the hemispherical average of potential temperature θ at a pressure level. Specifically, for the PV contour, the LWA_{q250} is defined as

$$LWA_{q250}(\lambda, \phi_e) = \frac{a}{\cos \phi} \left[\int_{q_e \geq 0, \phi \geq \phi_e} q_e(\lambda, \phi) \cos \phi d\phi - \int_{q_e \leq 0, \phi \leq \phi_e} q_e(\lambda, \phi) \cos \phi d\phi \right], \tag{2}$$

where ϕ_e is the equivalent latitude of q_{250} . $q_e(\lambda, \phi) = q(\lambda, \phi) - q_{250}(\phi_e)$, denoting the departure from Lagrangian-mean eddy-free reference state of PV. The LWA budget at a single level is formulated as follows:

$$\begin{aligned} -\frac{1}{a} \frac{\partial}{\partial \lambda} \left[u_{REF} A - \frac{a}{\cos \phi} \int_0^{\Delta \phi} u_e q_e \cos(\phi + \phi') d\phi + \frac{1}{2} \left(v_e^2 - u_e^2 - \frac{R}{H} \frac{e^{-z/H} \theta_e^2}{\partial \theta / \partial z} \right) \right] &= \frac{\partial}{\partial t} A \cos \phi = \\ \underbrace{\dots}_{\text{Zonal LWA flux convergence}} &+ \underbrace{\frac{1}{a \cos \phi} \frac{\partial}{\partial \phi'} (u_e v_e \cos^2(\phi + \phi')) - e^{-z/H} \cos \phi \frac{\partial}{\partial z} \left(\frac{f e^{-z/H} v_e \theta_e}{\partial \theta / \partial z} \right)}_{\text{Meridional eddy momentum flux divergence}} \tag{3} \\ &+ \underbrace{-a \int_0^{\Delta} \phi' e^{z/H} \frac{\partial}{\partial z} \left(e^{-z/H} \frac{Q_e / c_p e^{\kappa z / H}}{\partial \theta / \partial z} \right) \cos(\phi + \phi') d\phi'}_{\text{Diabatic heating}} + \underbrace{Res}_{\text{Residual}} \end{aligned}$$

where A represents the local wave activity for simplicity. The physical meaning of each term on the right-hand side of the equation is elaborated as follows.

- The zonal LWA flux convergence is the sum of the zonal advection of LWA by background reference flow u_{REF} , eddy LWA flux convergence due to zonal Stokes drift and the zonal eddy momentum flux convergence. The sum of LWA advection by u_{REF} and zonal eddy momentum flux convergence are approximately proportional to the group propagation of the Rossby

waves in the reference state, and the zonal Stokes drift term represents nonlinear modification of the flux by large-amplitude waves. For the perturbation with small amplitude, the advection of LWA by reference state is dominant. For the perturbation with finite amplitude, the eddy LWA flux by zonal Stokes drift prevails over the other two terms, leading up to the ‘‘traffic jam effect’’ for blocking in Nakamura and Huang (2018). Basically, the zonal LWA flux convergence manifests the contribution from the horizontal wave train and horizontal advection of wave activity.

- The meridional eddy momentum flux divergence manifests the contribution due to the meridional redistribution of momentum by waves.
- The meridional eddy heat flux difference represents the baroclinic eddy generation from lower levels and the vertical propagation of the eddy activity. It is often associated with local transient eddy feedback resultant from baroclinic eddy generation.
- The last two terms denote the contribution from diabatic heating and residual term including wave dissipation due to irreversible PV mixing from wave breaking, ageostrophic components and possible errors of budget.

In summary, Eq. (3) provides a feasible diagnostic framework to quantify the role of Rossby wave train, wave activity advection, local baroclinic eddy generation and diabatic heating in determining the dynamical evolution of cut-off lows. The detailed derivation of each budget term and physical meaning can be referred to Huang and Nakamura (2017) and Wang et al. (2021).

2.4 Diagnostics of horizontal wave propagation

To investigate the wave propagation associated with the cut-off low evolution, we also diagnose the horizontal component of the wave activity flux derived by Takaya and Nakamura (2001), hereafter TN01:

$$W = \frac{p \cos \phi}{2|\bar{V}|} \left\{ \frac{\bar{U}}{a^2 \cos^2 \phi} \left[\left(\frac{\partial \Psi'}{\partial \lambda} \right)^2 - \Psi' \frac{\partial^2 \Psi'}{\partial \lambda^2} \right] + \frac{\bar{V}}{a^2 \cos \phi} \left[\frac{\partial \Psi'}{\partial \lambda} \frac{\partial \Psi'}{\partial \phi} - \Psi' \frac{\partial^2 \Psi'}{\partial \lambda \partial \phi} \right] \right\}, \tag{4}$$

where Ψ' denotes the transient geostrophic stream function which is calculated as the deviation of the stream function from the daily climatology, \bar{U} and \bar{V} are the climatological background flow. The wave activity flux can quantify the propagation of transient eddies in accordance with the background flow, with its direction parallel to the local group

velocity of Rossby waves. Alternatively, we can identify the variations of source/sink of wave packet and the wave energy propagation relative to/in accordance with the mean flow associated with the cut-off lows.

2.5 Zonal momentum budget

To quantify contributions of different dynamical processes to the change of zonal wind associated with cut-off lows, we employ the zonal momentum budget (Eq. (2.24) in Holton (2004)):

$$\frac{\partial u}{\partial t} = f v_a - (\mathbf{V} \cdot \nabla) u, \quad (5)$$

where $\frac{\partial u}{\partial t}$ denotes the zonal wind tendency, v_a is the ageostrophic component of the meridional wind, and \mathbf{V} is the three-dimensional wind vector. The physical meaning of each term on the right side is elaborated as follows: the ageostrophic acceleration associated with meridional overturning circulation and advection by the horizontal flow. In our study, the composite mean of each term in Eq. (5) over the cut-off low period is investigated to reveal roles of distinct processes in determining the evolution of zonal wind accompanied with cut-off lows. The total advection term in Eq. (5) can be further decomposed to three components $-(\mathbf{V} \cdot \nabla) u = -(\overline{\mathbf{V}} \cdot \nabla) \overline{u}' - (\mathbf{V}' \cdot \nabla) \overline{u} - (\mathbf{V}' \cdot \nabla) u'$, where overbar denotes the daily climatology and prime denotes the anomalous field relative to the daily climatology. Therefore, the total advection term can be attributed to advection of anomalous momentum by mean flow, advection of mean momentum by anomalous flow and advection of anomalous momentum by anomalous flow.

2.6 Thermal budget

To help understand the local temperature evolution associated with the cut-off low, we also apply the thermal budget analysis. Specifically, the rate of temperature change at a given point in the atmosphere is governed by the thermodynamic equation, which we present below:

$$\frac{\partial T}{\partial t} = -\mathbf{V}_h \cdot \nabla_h T + \omega \left(\kappa \frac{T}{p} - \frac{\partial T}{\partial p} \right) + \frac{Q}{c_p}, \quad (6)$$

where T is the temperature, \mathbf{V}_h is the horizontal wind vector, ∇_h denotes the horizontal gradient operator, ω is the vertical velocity in pressure coordinates, c_p is the specific heat capacity of air at constant pressure, R_d is the gas constant for dry air, $\kappa = R_d/c_p$, and Q is the diabatic heating. By Eq. (6), the local change of temperature is the sum of the horizontal advection of temperature, changes in temperature due to

adiabatic expansion or compression due to vertical motion, and diabatic processes.

3 Dynamical evolution of cut-off lows

Figure 2 examines the evolution of anomalous 250-hPa circulation and wave propagation properties associated with the cut-off low evolution. The left column of Fig. 2 shows the lagged composites of anomalous Z_{250} and TN01 wave activity flux against the cut-off low index. Preceding the onset of cut-off lows by 3–6 days (Fig. 2a), the Z_{250} displays alternating positive and negative anomalies from high-latitude North Atlantic to Northeast Asia. It is characterized with a cyclonic anomaly in the subpolar North Atlantic, an anticyclonic anomaly in the Ural region and a cyclonic anomaly in the Northeast Asia. The anomalous wave activity flux shows a Rossby wave packet originating from the subpolar North Atlantic and propagating downstream toward the Northeast Asia with a curved path, suggesting an important role of Rossby wave train in the initial formation of a cyclonic low.

Then at lags – 2 to – 1 days, the Z_{250} exhibits much stronger negative anomalies in the trough center and positive anomalies to the northwest of the trough (Fig. 2b), suggesting a rapid growth of the preexisting cyclonic low. The anomalous wave activity flux displays a weaker horizontal wave propagation in the Eurasian continent, suggesting the incoming Rossby wave packet from the remote North Atlantic diminishes at this stage. Instead, significant eastward wave packets are found around the trough center.

Following the onset of cut-off lows by 0–4 days (Fig. 2c), the strong negative Z_{250} anomalies in the trough center are weakened gradually and move downstream. Stronger wave train emanates from the cut-off low region to the North Pacific, which may disperse the eddy energy within the cut-off low region. The role of planetary wave activity flux in the cut-off low life cycle is similar to the blocking evolution in Nakamura (1994) that the local absorption of the wave activity and its reemission, in association with temporary “obstruction of Rossby wave propagation”, contribute to the formation and the following decay of the blocking.

The right column of Fig. 2 further displays the evolution of LWA_{q250} for comparison. At lags – 6 to – 3 days, as shown in Fig. 2d, the LWA shows positive anomalies in the Ural region and negative anomalies in the subpolar North Atlantic and Northeast Asia, consistent with the geopotential height anomalies shown in Fig. 2a. At lags – 2 to – 1 days, the local wave activity shows strong positive anomalies over a broader area from the Ural to the Northeast Asia (60°–130° E, 40°

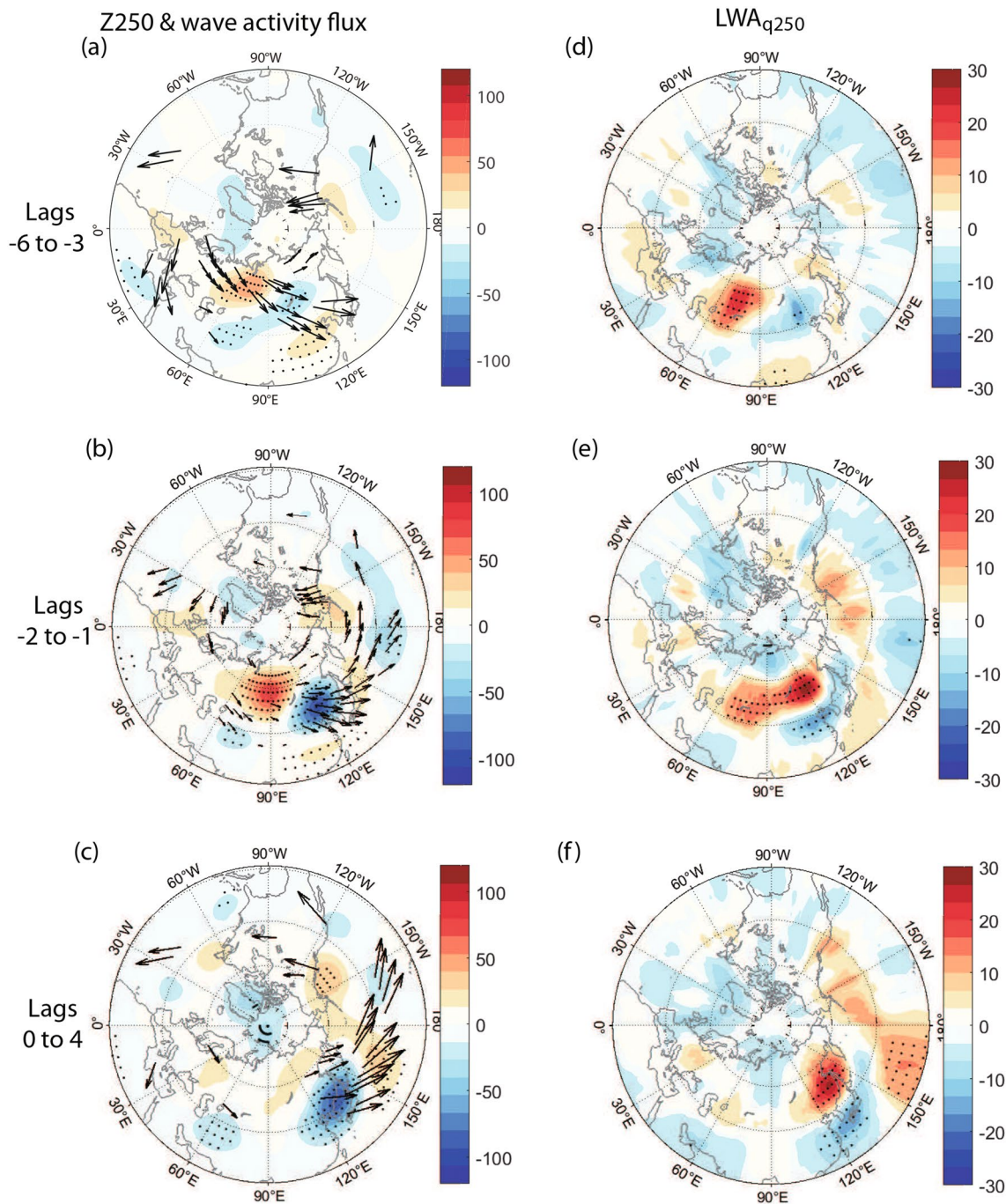


Fig. 2 (Left) Lagged composites of the anomalous Z_{250} (shading in m) and corresponding wave activity flux of TN01 (arrows, unit: $\text{m}^2 \text{s}^{-1}$) for strong cut-off lows over Northeast Asia in early summer. Here only the significant fluxes at the 70% confidence level are plot-

ted. (Right) as in (left) but for the LWA_{q250} anomaly (shading in ms^{-1}). Values that are significant at the 95% confidence level using a two-tailed t test are highlighted with black dots

-60°N), suggesting strong local wave activity anomalies in both the cut-off low region and its upstream (Fig. 2e). At lags 0–4 days, the positive anomalies of LWA move downstream toward the North Pacific (Fig. 2f).

To explicitly understand the evolution of local wave activity, we diagnose the time sequence of the LWA budget at 250 hPa associated with cut-off lows. Figure 3 displays composites of the $115^\circ\text{--}145^\circ \text{E}$ zonally averaged LWA anomaly and

its budget as a function of time from lags -6 to $+6$ days. The LWA shows significant positive anomalies between 40° and 60° N from lags -3 to $+5$ days and exhibits slightly southward movement (Fig. 3a). The LWA anomaly is already positive before the onset of cut-off lows, suggesting that there is already a cyclone in the cut-off low region before the onset. To explain the positive LWA anomaly, we diagnose the evolution of each component of LWA budget in Eq. (3). As shown in Fig. 3b, the LWA shows positive tendency at short negative lags and negative tendency at positive lags. Decomposition of LWA tendency shows that the positive LWA tendency at negative lags is mostly contributed by the zonal LWA flux convergence (Fig. 3c) and the eddy heat flux differential (Fig. 3e), suggesting the importance of zonal advection of LWA and local baroclinic eddy generation in the formation of cut-off lows. The decay of LWA at positive lags is dominantly due to the changes of zonal LWA flux convergence.

Based on the above diagnosis, we divide the life cycle of Northeast Asian cut-off lows into three stages: initial formation (lags -6 to -3 days), rapid amplification (lags -2 to -1 days) and decay stages (lags $0-4$ days). We next diagnose the LWA budget at each stage to further understand the mechanism responsible for the cut-off low evolution. Figures 4, 5 and 6 display the lagged composites of each budget term (Eq. (3)) during these three stages. At lags -6 to -3 days (Fig. 4), the LWA tendency shows minor changes. There is a counteract effect between the zonal LWA flux convergence anomalies (Fig. 4b) and the eddy heat flux differential anomalies (Fig. 4d) along the high-latitude wave train path shown in Fig. 2a, indicating a baroclinic signature of the Rossby wave train. This wave train helps feed the large zonal LWA flux in the amplification stage that will be discussed shortly.

At lags -2 to -1 days (Fig. 5), the LWA tendency shows significantly positive anomalies in the cut-off low region, suggesting rapid enhancement of wave activity there. Decomposition of LWA tendency shows that such positive anomalies mostly result from the large zonal LWA flux convergence (Fig. 5b) and the eddy heat flux differential (Fig. 5d), with the former mainly contributing to the east of 120° E and the latter contributing to the west of 120° E. Further decomposition of zonal LWA flux convergence shows that the LWA advection by reference flow plays a dominant role at this stage, and the zonal Stokes shift term acts to modulate the zonal LWA flux capacity and help amplify the cyclonic low (Figs. S2 and S3), which is consistent with the results of Nakamura and Huang (2018). This suggests that both the zonal advection of LWA flux from upstream and local eddy generation play important roles in amplifying the positive LWA anomalies in the cut-off low region. Therefore, both barotropic and baroclinic processes are indispensable for the cut-off low development. We also note that the

meridional eddy momentum flux divergence and residual term may play a secondary role to the positive LWA anomalies west of 120° E.

At lags $0-4$ days (Fig. 6), the local tendency of LWA shows negative anomalies in the cut-off low region, suggesting a decay of the cut-off low. Through the LWA budget diagnosis, we find that the decay of LWA is mainly attributed to the zonally LWA flux convergence (Fig. 6b), although the decay rate is slightly slowed down by the local baroclinic eddy generation (Fig. 6d) and meridional eddy momentum flux divergence (Fig. 6c).

4 Modulation of background flow on the wave propagation and eddy generation

4.1 Climatology of background flow

To further understand the behaviors of wave propagation, energy accumulation and dispersion in different stages of cut-off low evolution, we next examine the background circulation associated with cut-off lows because those wave properties are often organized by the background flow (Hoskins and Karoly 1981; Seager et al. 2003; Barnes and Hartmann 2011). Figure 7 reviews key aspects of the climatological mean circulation fields over the Northeast Asia during the early-summer months of May and June. As Rossby wave propagation requires wave phase speed less than background zonal wind, and westerly jet could act as a wave guide (Seager et al. 2003; Nakamura and Huang 2018), we first examine the zonal wind climatology in Fig. 7a. The climatological zonal wind at 250 hPa (shading) displays a clear split-jet structure over Eurasian continent, with a mid-latitude jet centered at 60° N extending from North Europe to Northeast Asia and a subtropical jet extending from North Africa to North Pacific. The Northeast Asia is exactly at the midlatitude jet exit to the north of the subtropical jet (black box in Fig. 7a), which is favorable for the formation of a cyclonic wind anomaly. The zonal wind diffuence at the midlatitude jet exit also helps keep the zonal LWA flux capacity small and thus is easier for the zonal LWA flux to reach its maximum (Nakamura and Huang 2018). Indeed, the climatological large LWA (blue contour) is found exactly at the exit region of the midlatitude jet (blue contour in Fig. 7a). The spatial configurations of climatological midlatitude jet and subtropical jet may also help explain that the Northeast Asian cut-off lows are more common in early summer than in mid summer (June and August). During mid summer, the midlatitude jet in the western Eurasian almost disappears, and the subtropical jet over East Asia is weaker and moves westward, which is not in favor of

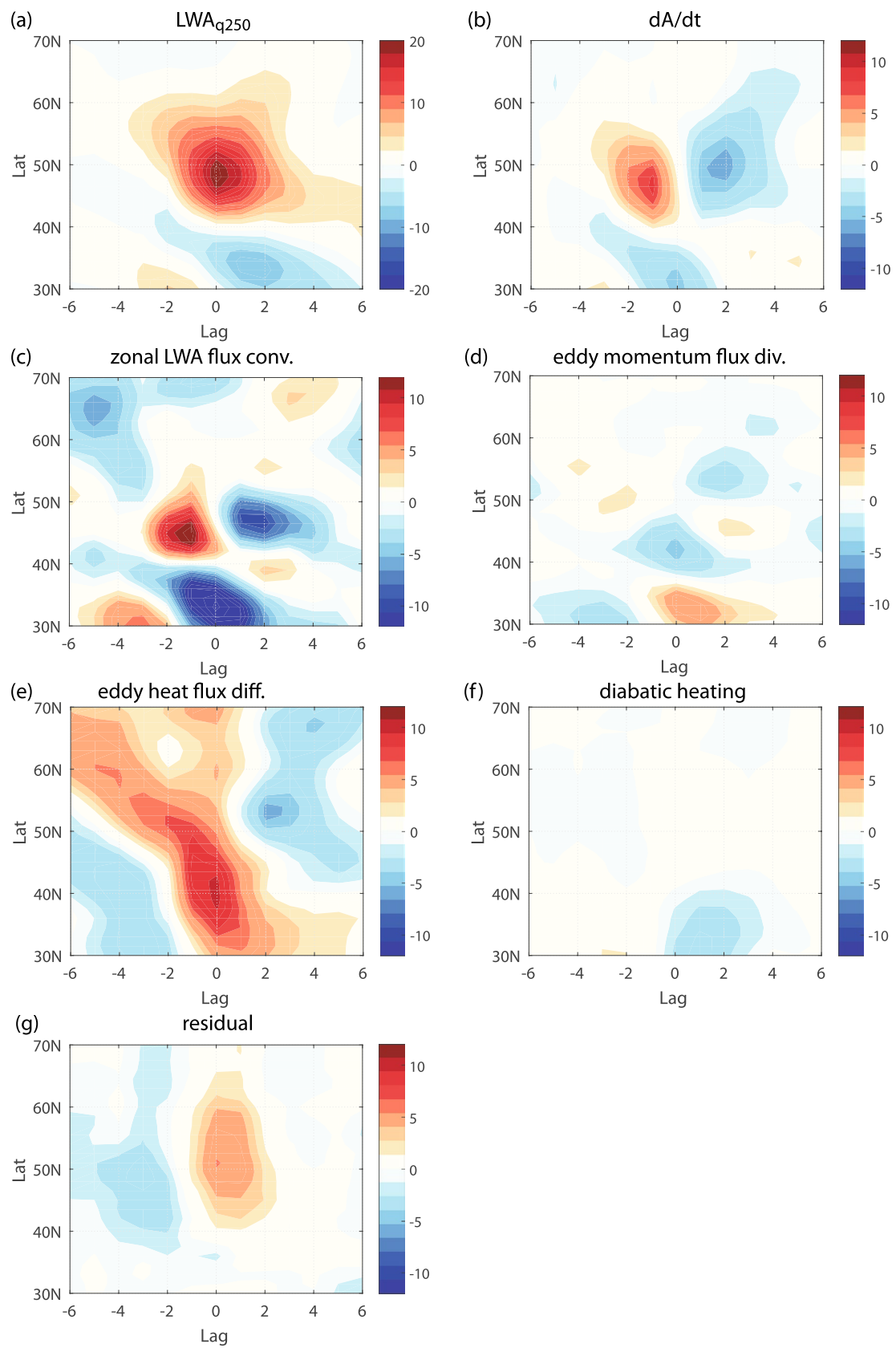


Fig. 3 Time-latitude Hovmöller plot of the 115° – 145° E zonally averaged LWA_{q250} anomaly and its budget (Eq. (3)) for positive phase of cut-off low index. **a** $LWA_{q250} \cos \phi$ (unit: ms^{-1}), **b** wave activity net tendency, **c** zonal LWA flux convergence, **d** meridional eddy momentum flux divergence, **e** meridional eddy heat flux difference, **f** diabatic heating and **g** residual. The unit of (b–g) is $ms^{-1} day^{-1}$

frequent formation of cyclonic anomalies and cut-off lows in Northeast Asia (Fig. S4). It is also important to note that, the summer monsoon begins to affect the Northeast Asia during

mid summer, and thus may play a role in affecting cut-off lows during mid summer.

As suggested by Luo et al. (2018, 2019), the wave propagation and energy dispersion are strongly dependent on the background meridional gradient of potential vorticity. As shown in Fig. 7b, the climatological PV gradient display two clear zonally-oriented branches, with one located in the high latitude around 60° N and the other located in subtropics extending from North Africa to North Pacific. The Northeast Asia is located between the two branches, exhibiting a PV gradient minimum, and thus is not in favor for horizontal

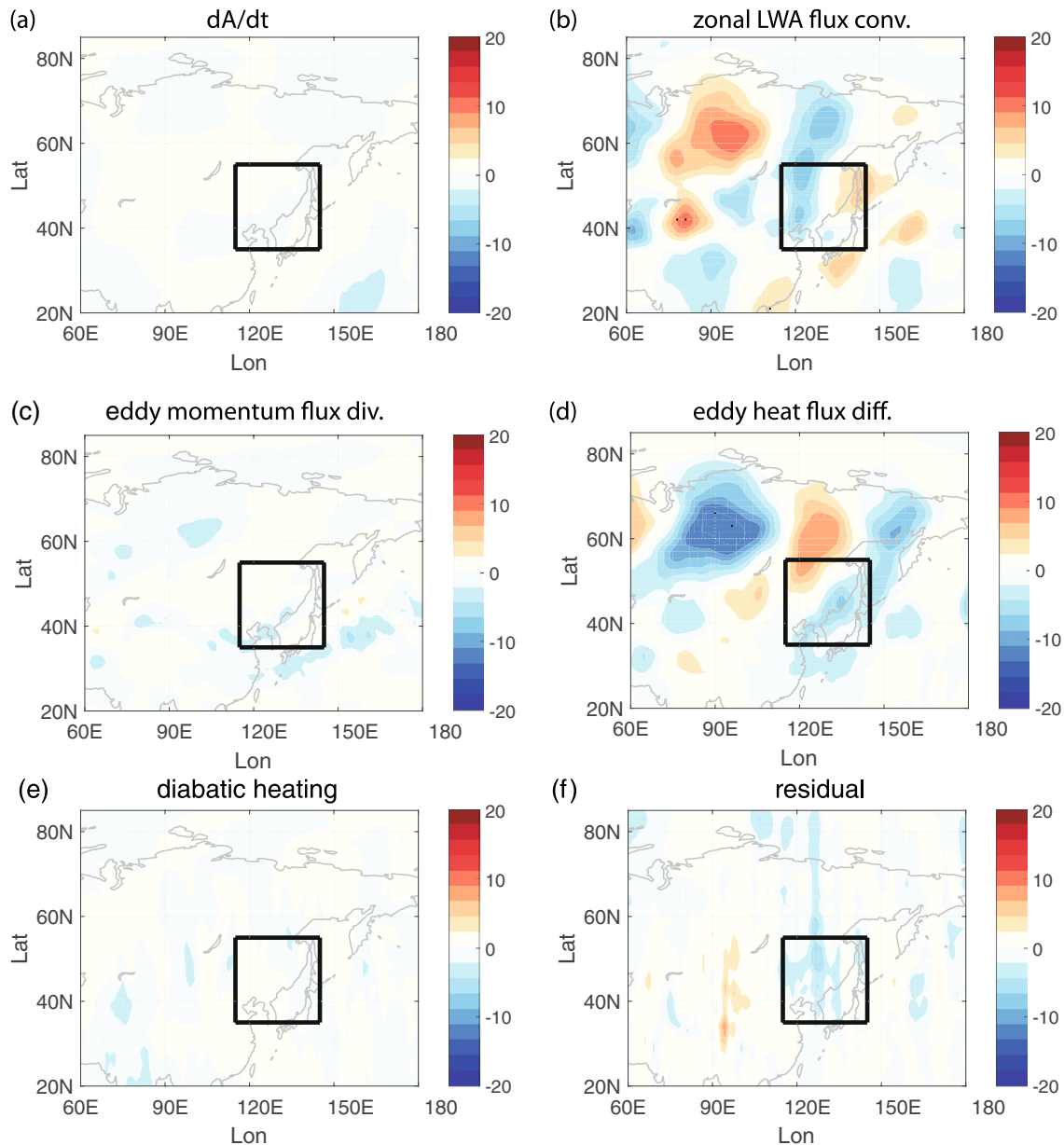


Fig. 4 Lagged composites of wave activity budget terms at lags -6 to -3 days. **a** Wave activity net tendency, **b** zonal LWA flux convergence, **c** meridional eddy momentum flux divergence, **d** meridional

eddy heat flux difference, **e** diabatic heating and **f** residual. The unit of (a–f) is $ms^{-1} day^{-1}$. Values that are significant at the 95% confidence level using a two-tailed t test are highlighted with black dots

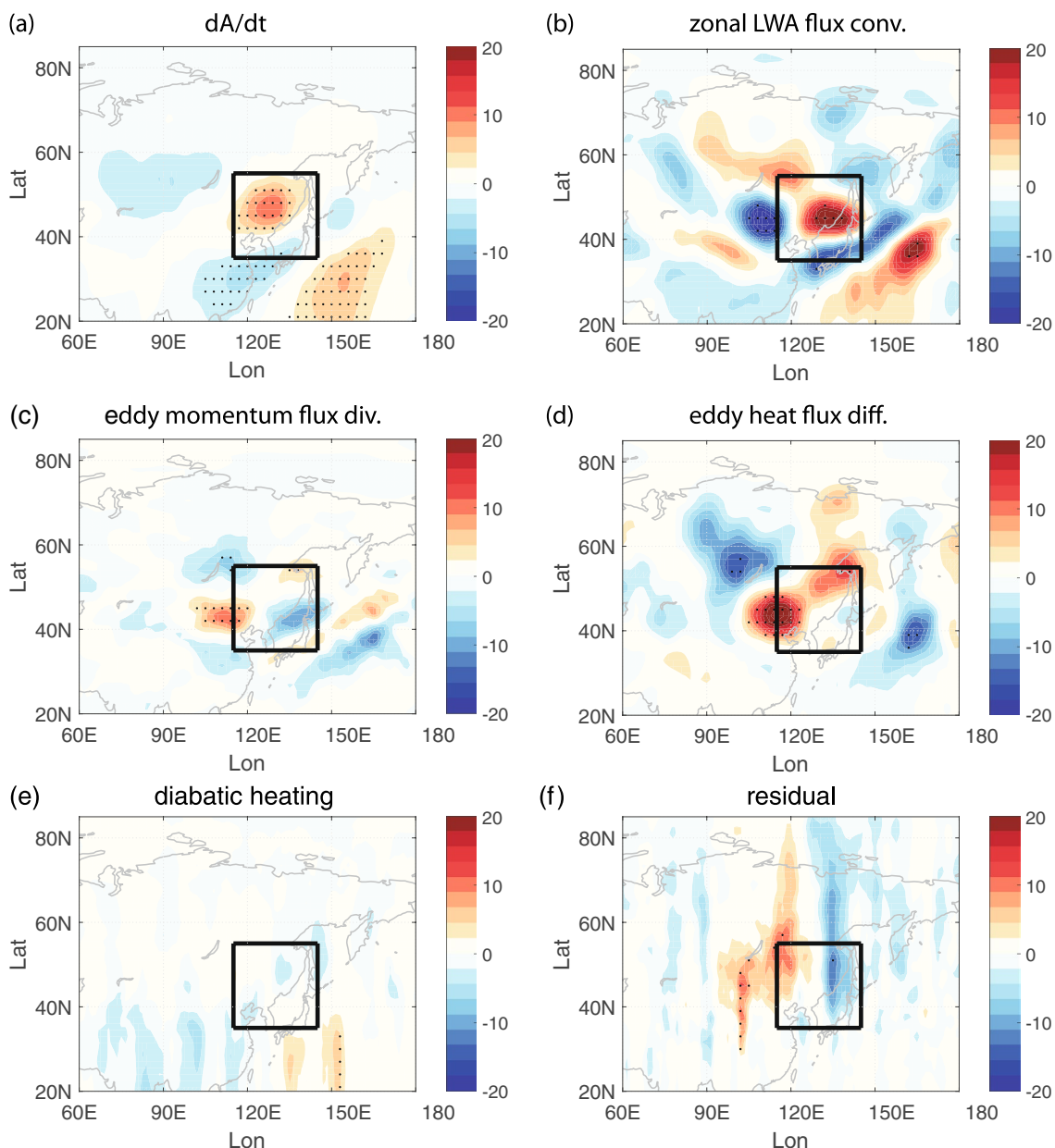


Fig. 5 As in Fig. 4 but for averaged composites at lags -2 to -1 days

wave propagation toward downstream. Based on the linear baroclinic instability theory, the baroclinic eddy generation relies on the lower-tropospheric baroclinicity. Figure 7c shows the climatology of 850-hPa meridional temperature gradient ($-dT/dy$). The Northeast Asia is in a weak temperature-gradient spot between the two branches of large temperature gradient in the high latitude and subtropics, and thus the local eddy growth is relatively weak. When the wave packets in the Eurasian continent pass through Northeast Asia, the locally weak PV gradient and weak low-level baroclinicity there will prohibit the wave packets proceeding downstream and thus assist in local energy accumulation. To

conclude, the climatological geostrophic distribution of the jets, PV gradient and baroclinicity are in favor of the formation of cyclonic circulation and local energy accumulation in Northeast Asia.

4.2 Evolution of background flow associated with cut-off lows

The time evolution of background circulation anomalies associated with cut-off lows is then explicitly examined in Fig. 8. The left column of Fig. 8 displays the lagged composites of zonal wind and the TN01 wave activity flux

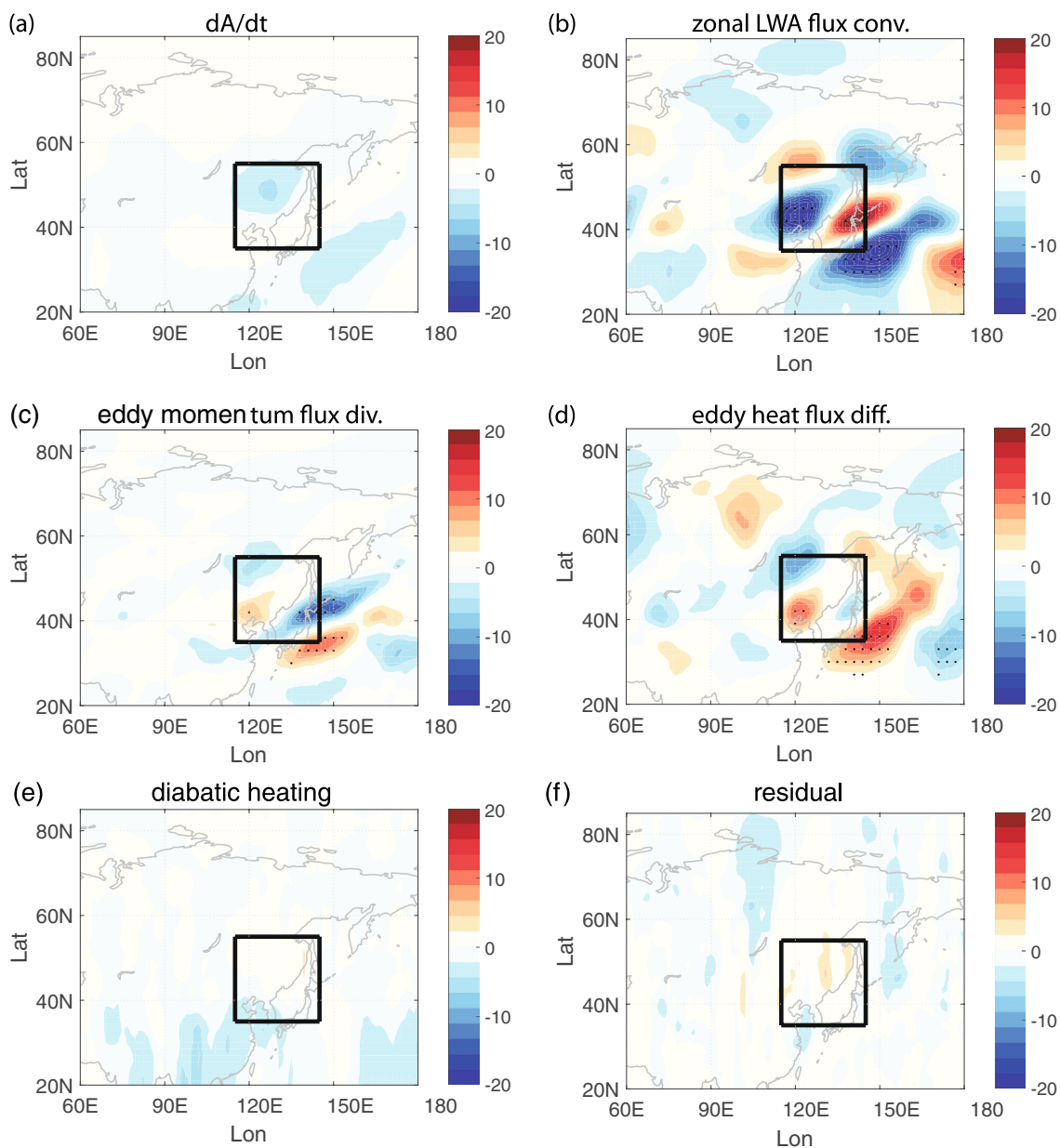


Fig. 6 As in Fig. 4 but for averaged composites at lags 0–4 days

anomalies. At lags – 6 to – 3 days (Fig. 8a), the zonal wind displays a split-jet structure in the Eurasian continent, with a midlatitude jet located northward of 60° N in western Eurasia and a subtropical jet located southward of 40° N from North Africa to North Pacific (similar to the climatological jet structure in Fig. 7a). The Rossby waves propagate eastward along the midlatitude jet over western Eurasia and then along the subtropical jet over East Asia (arrows). At lags – 2 to – 1 days (Fig. 8b), the zonal winds are decelerated at the exit of midlatitude jet (50°–60° N, 110°–130° E) and accelerated in the subtropical jet core. Accompanied by the decrease of the zonal wind speed at the midlatitude jet exit,

the midlatitude jet becomes more slow-moving and approximately stationary, which prevents the upstream wave packet proceeding downstream and thus favor more local energy accumulation in the Northeast Asia. Meanwhile, a newly developed Rossby wave packet propagates from the northern edge of the subtropical jet (40°–50° N, 120° E) to the western North Pacific (arrows). Such horizontal wave propagation further decelerates the zonal wind on the northward flank of subtropical jet but accelerates the zonal wind at the subtropical jet core, favoring further development of the preexisting cyclonic anomaly in the Northeast Asia and thus can be considered as a positive feedback to the mean flow.

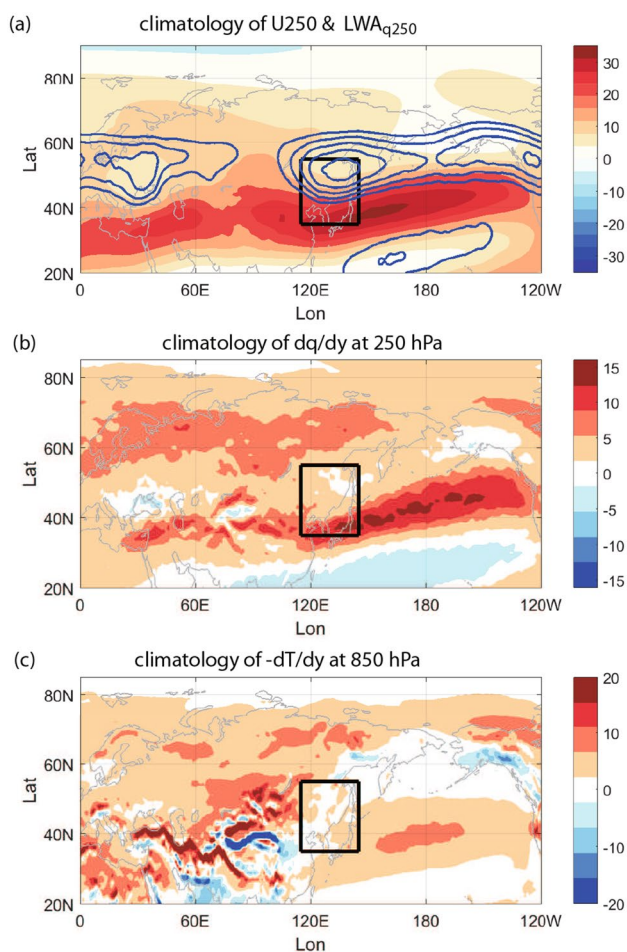


Fig. 7 Climatology of **a** zonal wind at 250 hPa (shading, ms^{-1}) and LWA_{q250} (blue contour, starting from 100 ms^{-1} with a contour interval of 10 ms^{-1}), **b** meridional PV gradient (dq/dy) at 250 hPa (day^{-1}), and **c** meridional temperature gradient ($-dT/dy$) at 850 hPa ($\text{K}(1000 \text{ km})^{-1}$). The black boxes denote the key region of cut-off lows (115° – 145° E, 35° – 55° N)

At lags 0–4 days, as shown Fig. 8c, the area of decelerated zonal wind to the north of the subtropical jet expands eastward, and thus the associated Rossby wave propagation also expands more eastward and diverts in the eastern Pacific.

The middle column of Fig. 8 displays the lagged composites of total field and anomalies of 250-hPa PV gradient. The total PV gradient contours show two zonal branches in all stages as that of climatology. The most significant changes of PV gradient anomalies are found from lags -2 to $+4$ days when a clear north-south dipole centering at 50° N appears (Fig. 8e, f). The northern lobe shows a strong reduction of PV gradient, inhibiting waves propagating eastward and favoring energy accumulation. The southern lobe exhibits strong increase of the PV gradient, which coincides with

the climatological PV gradient center in subtropics, and thus favoring more wave propagating toward the North Pacific.

The lagged composites of meridional temperature gradient at 850 hPa are shown in the right column of Fig. 8. Significant changes of lower-tropospheric baroclinicity emerge from lags -2 to -1 days (Fig. 8h), manifesting as an increased baroclinicity in the south and a decreased baroclinicity in the north, which is consistent with the dipolar spatial pattern of the zonal wind and PV gradient changes. Positive anomalies of temperature gradient in the southern lobe is favorable for more eddy generation, and thus helps explain the positive eddy heat flux differential anomalies there in Fig. 5d. These results demonstrate that in addition to the zonal advection and propagation of wave activity from the upstream side, the local baroclinic eddy generation due to changes in background temperature gradient also plays a role in the amplification of cut-off lows.

Based on the above diagnostic analyses, we propose a dynamical mechanism for the formation of Northeast Asian cut-off lows. A Rossby wave packet originating from the subpolar North Atlantic propagates along the Eurasian mid-latitude jet, which initializes the formation of a cyclonic anomaly over the Northeast Asia. Then the zonal winds are decelerated at the exit of midlatitude jet and accelerated in the East Asian subtropical jet core. Such changes of background flow favor more energy accumulation through the zonal advective flux of wave activity from the upstream side and more baroclinic eddy generation below the subtropical jet. These two processes work together to let the preexisting cyclonic anomaly growing rapidly over the Northeast Asia.

4.3 Possible reason for background flow changes

Since the changes of background zonal wind can modulate the wave propagation and eddy generation which are important for the cut-off low amplification, we next explore the causes for the wind anomalies. Similar to the method in Chan et al. (2020), we quantify the relative contributions of different dynamical processes (i.e., ageostrophic acceleration and zonal flow advection) by diagnosing the zonal momentum budget in Eq. (5). Figure 9 shows the composites of each component in the zonal momentum budget at lags -2 to -1 days. The first-order balance is between the ageostrophic acceleration (Fig. 9a) and the zonal flow advection (Fig. 9b). Comparison between Figs. 8b, 9 shows that the advection term makes the dominant contribution to the zonal wind anomaly during the amplification stage of the cut-off low s.

The importance of the advection term is further understood by decomposing it into three components: mean flow advection of anomalous momentum, anomalous flow advection of mean momentum and anomalous flow advection of

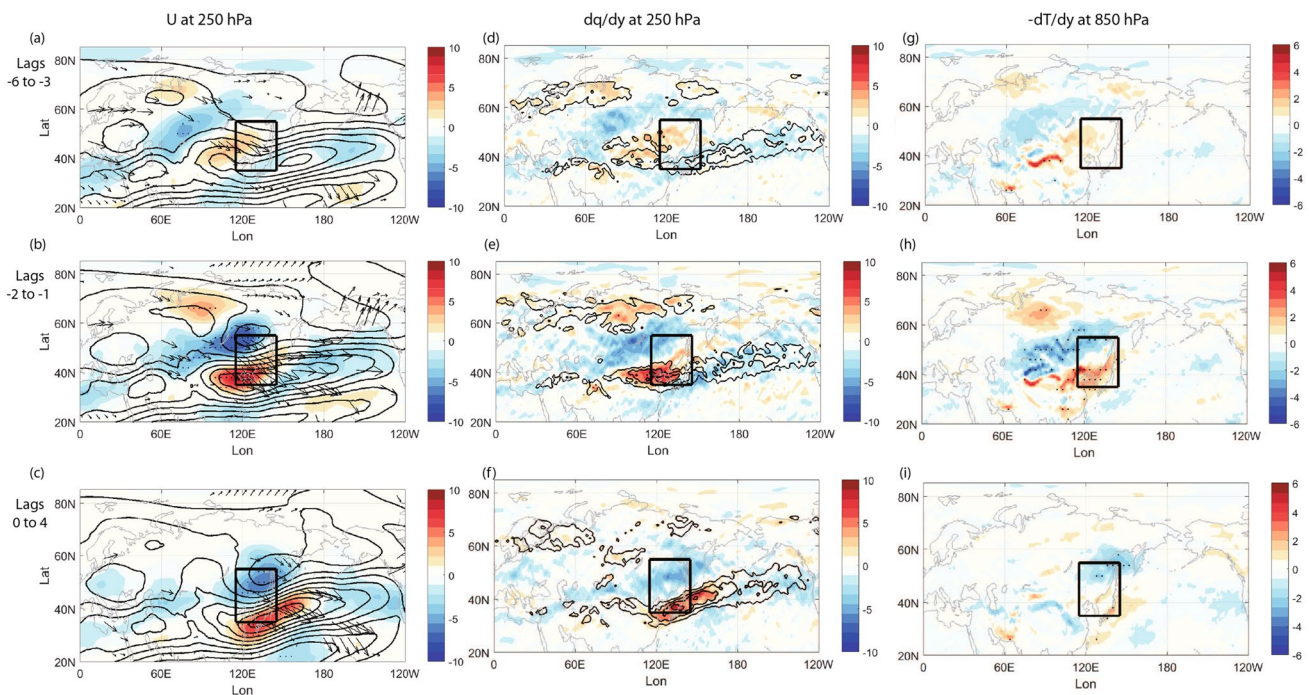


Fig. 8 Lagged composite maps of (left) the 250-hPa zonal wind (contour with interval of 5 ms^{-1} starting from 5 ms^{-1}) and zonal wind anomaly (shading, ms^{-1}), wave activity flux anomaly of TN01 (arrows), (middle) the 250-hPa meridional PV gradient (contour with interval of $4 \text{ day}^{-1} (1000 \text{ km})^{-1}$ starting from $8 \text{ day}^{-1} (1000 \text{ km})^{-1}$)

and its anomaly (shading, $\text{day}^{-1} (1000 \text{ km})^{-1}$), and (right) the meridional temperature gradient ($-\text{dT}/\text{dy}$) anomaly at 850 hPa ($\text{K} (1000 \text{ km})^{-1}$). Values that are significant at the 95% confidence level are highlighted with black dots

anomalous momentum. Figure 10 shows the composites of these components at lags -2 to -1 days. Comparison between Figs. 9b, 10 illustrates that the advection is mainly attributed to the anomalous zonal momentum advected by the mean flow. And the mean zonal flow advection dominates over the mean meridional flow advection (results not shown). To conclude, the background zonal wind changes is predominantly driven by the mean flow advection of anomalous zonal momentum.

We next explore the reason for the changes of background temperature gradient, as it also plays a role in amplifying cut-off lows through baroclinic eddy generation (Fig. 8h). Figure 11 shows the 2-day averaged composite maps of the anomalous 850-hPa temperature budget (Eq. (6)) before the peak days of the cut-off low index. Comparison between Fig. 11a–d illustrates that changes of lower-tropospheric temperature are mainly contributed by the horizontal temperature advection (Fig. 11b). The adiabatic term helps to bring cold anomaly to the coastal East Asia (Fig. 11c). The diabatic heating plays a damping role (Fig. 11d, e). Similar to the zonal wind change, the total

horizontal advection of temperature is mainly determined by the mean flow advection on anomalous temperature (figures not shown). Therefore, through the above analyses, we conclude that both the background zonal wind and temperature are evolved mainly through the horizontal advection of anomalous fields by mean flow.

5 Conclusions and discussions

In Northeast Asia, strong precipitation and persistent cool weather are strongly affected by cut-off lows during early summer. Despite the severe weather impact of cut-off lows, the mechanism responsible for their life cycles has less been explored. This study proposes a dynamical mechanism for the early-summer cut-off low evolution through the local finite-amplitude wave activity budget analysis. As summarized in Fig. 12, a Rossby wave train from the subpolar North Atlantic initializes a cyclonic anomaly in Northeast Asia. Then the zonal LWA flux convergence

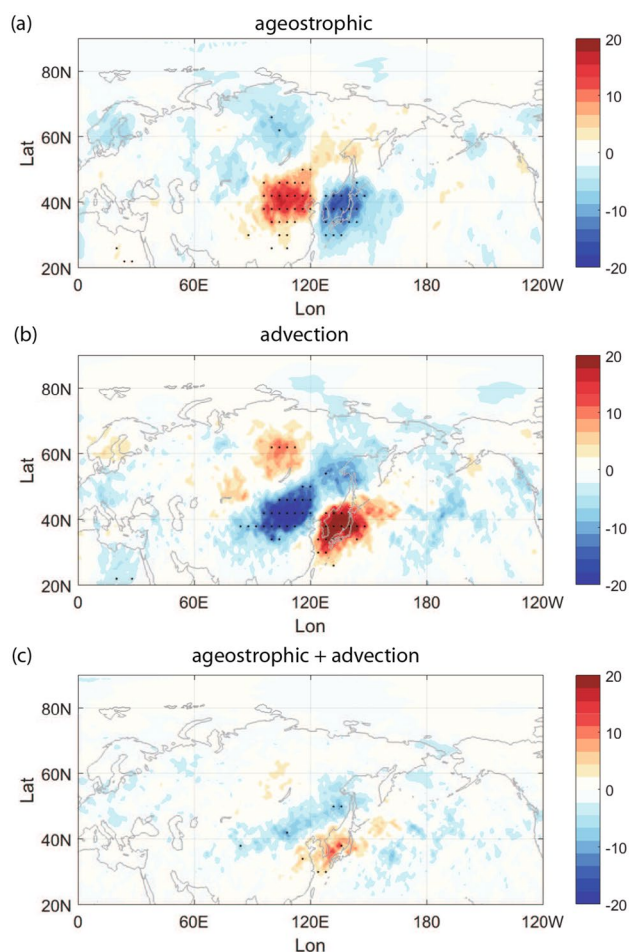


Fig. 9 2-day averaged composites of the zonal momentum budget (Eq. (5) at 250 hPa, with unit of $\text{ms}^{-1} \text{day}^{-1}$) at lags -2 to -1 days. Shown maps are **a** ageostrophic acceleration, **b** horizontal advection, and **c** summation of ageostrophic acceleration and advection. Values that are significant at the 95% confidence level are highlighted with black dots

and local baroclinic eddy generation act to amplify the cyclonic anomaly rapidly, forming a cut-off low. The cut-off low is eventually decayed through the energy disperse by the zonal LWA flux convergence.

Furthermore, we argue that changes of background flow play an important role in modulating such wave propagation and eddy generation. Preceding the cut-off low onset by 3–6 days, the wave train propagates along the midlatitude jet in western Eurasia and subtropical jet in East Asia. Then the zonal wind is decelerated at the exit of midlatitude jet and accelerated in the subtropical jet core. Such changes of zonal wind prevent the incoming midlatitude wave packet proceeding downstream but favor

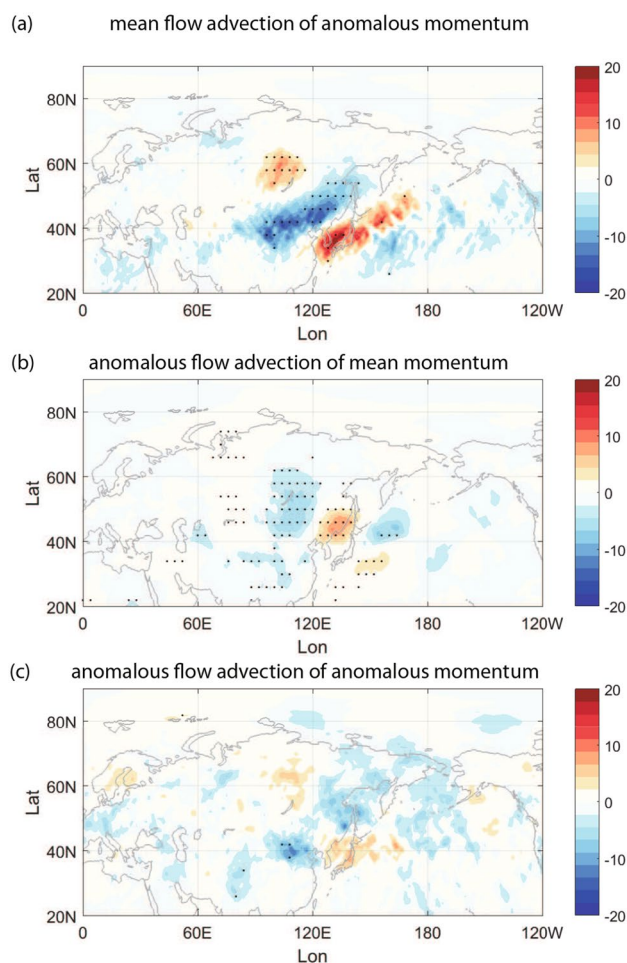


Fig. 10 As in Fig. 9 but for the momentum advection budget. Shown maps are the composites of **a** mean flow advection of anomalous momentum, **b** anomalous flow advection of mean momentum and **c** anomalous flow advection of anomalous momentum

more local eddy generation below the subtropical jet, and thus act to reinforce the preexisting cyclonic anomalies. This is similar to the study of O'Reilly et al. (2016) that a quasi-stationary development of midlatitude jet is efficient for lower-tropospheric meridional eddy heat transport to amplify the European blocking. Utilization of the zonal momentum budget diagnostic, we further attribute the background zonal wind changes to the mean flow advection of anomalous zonal momentum. Through thermal budget analyses, we also show that local changes of lower-level temperature anomalies affecting the baroclinic eddy generation are dominantly attributed to the temperature advection by horizontal winds.

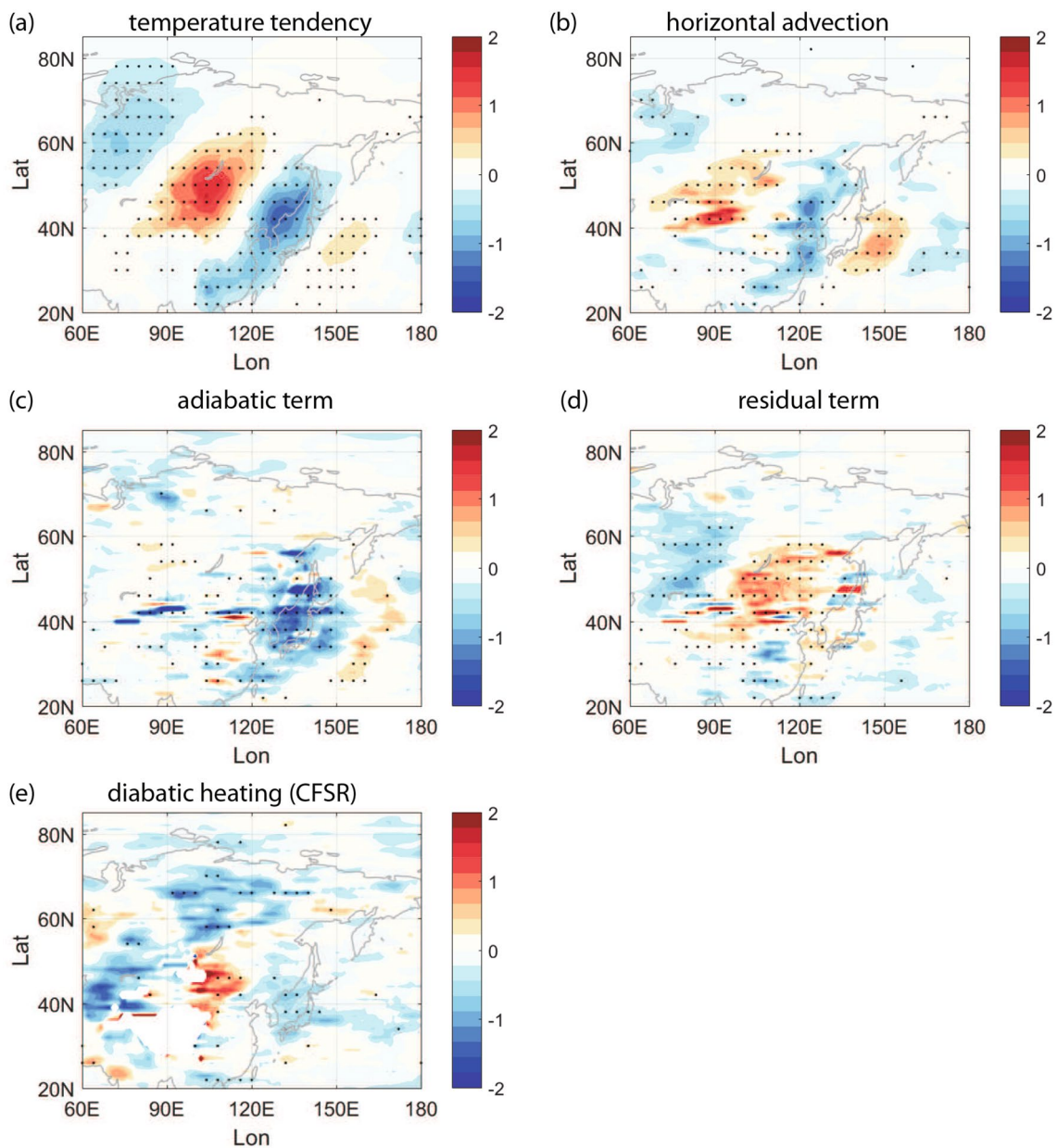


Fig. 11 2-day averaged composite maps of the temperature budget anomaly before the peak of cut-off low index. **a** Temperature tendency, **b** horizontal advection of temperature, **c** adiabatic term due to vertical motion, **d** residual term of the thermodynamical equation

and **e** diabatic heating output from CFSR dataset. The unit of (a–e) is K day^{-1} . Values that are significant at the 95% confidence level are highlighted with black dots

Our LWA budget analysis comprehensively depicts the wave activity evolution associated with cut-off lows, taking into account of the horizontal Rossby wave propagation, wave activity advection, local baroclinic eddy generation, as well as diabatic heating. This provides a framework to compare the relative importance of the individual process

outlined by previous studies Xie and Bueh (2015), Lin and Bueh (2021) in the cut-off low evolution. We highlight the important roles of regional eddy-mean flow interactions in the formation of cut-off lows and background flow in modulating the regional eddy-mean flow interactions. We also note that many other factors such as the water

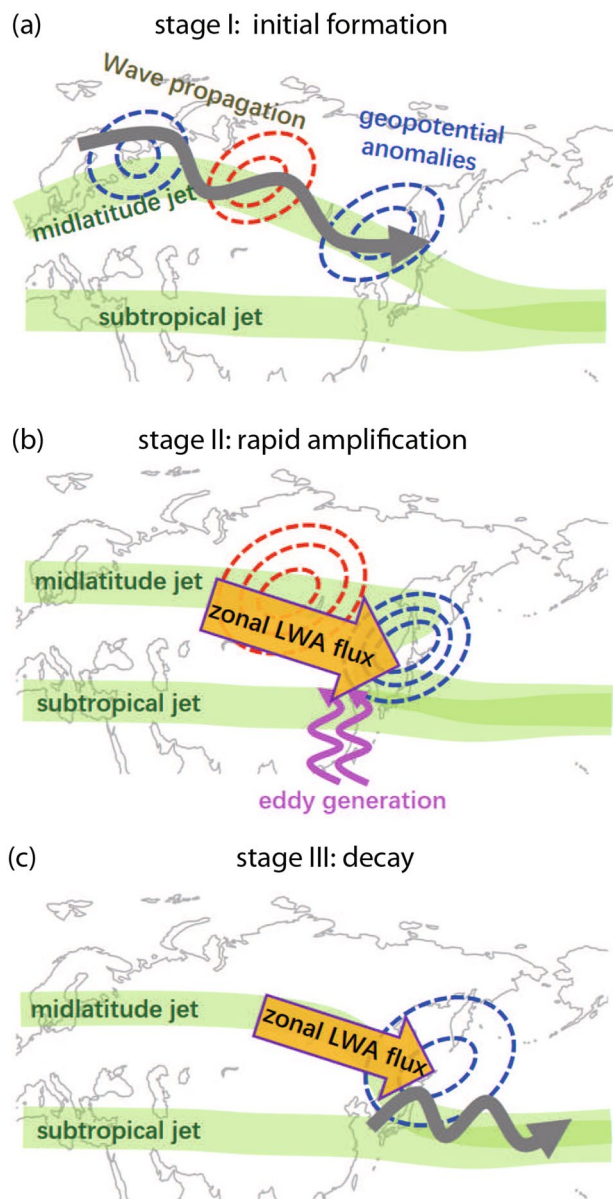


Fig. 12 A schematic diagram illustrating the dynamical mechanism for the evolution of early-summer cut-off lows over Northeast Asia. **a** Stage I: initial formation of cyclonic anomaly triggered by Rossby wave propagation along the Eurasian midlatitude jet. **b** Stage II: the background zonal winds are decelerated at the midlatitude jet exit and accelerated at the subtropical jet center, which favors more zonal LWA flux advection from the upstream and more eddy generations below the subtropical jet. The two processes work together to reinforce the preexisting cyclonic anomaly rapidly. **c** Stage III: horizontal propagation and advection of wave activity from the cut-off low region to the North Pacific disperse the energy and decay the cut-off lows. The thick green lines denote the midlatitude jet and the subtropical jet. The dashed contours denote the Z_{250} anomalies and the gray squiggles denote anomalous horizontal wave propagation. The bold orange arrow indicates the zonal LWA flux and the vertical arrows denote the vertical eddy propagation

vapor transport, subtropical high over western Pacific, remote influence from tropical convection, and even the stratosphere-troposphere interaction (Liu et al. 2013) may operate in the mechanisms for subseasonal variability of cut-off lows. These topics deserve further studies. A follow-up work is carried out to further delineate how the wave sources in the subpolar North Atlantic can generate low-frequency Rossby wave train by using a simplified model as in Chen et al. (2022), which may help to improve the subseasonal prediction of the Northeastern Asian cut-off lows and extreme precipitation.

Supplementary Information The online version contains supplementary material available at <https://doi.org/10.1007/s00382-022-06371-5>.

Acknowledgements This work was jointly supported by the National Key Research and Development Program of China (2021YFA0718000), Strategic Priority Research Program of Chinese Academy of Sciences under grant XDA2010030804 and NSF of China under Grants 42175075, 41975102. We are grateful to three anonymous reviewers, whose comments and suggestions have greatly improved the manuscript.

Data availability The ERA5 reanalysis is available at <https://www.ecmwf.int/en/forecasts/datasets/reanalysis-datasets/era5>. The CFSR data is available at <https://climatedataguide.ucar.edu/climate-data/climate-forecast-system-reanalysis-cfsr>.

Declarations

Conflict of interest The authors have no relevant financial or non-financial interests to disclose.

Open Access This article is licensed under a Creative Commons Attribution 4.0 International License, which permits use, sharing, adaptation, distribution and reproduction in any medium or format, as long as you give appropriate credit to the original author(s) and the source, provide a link to the Creative Commons licence, and indicate if changes were made. The images or other third party material in this article are included in the article's Creative Commons licence, unless indicated otherwise in a credit line to the material. If material is not included in the article's Creative Commons licence and your intended use is not permitted by statutory regulation or exceeds the permitted use, you will need to obtain permission directly from the copyright holder. To view a copy of this licence, visit <http://creativecommons.org/licenses/by/4.0/>.

References

- Barnes EA, Hartmann DL (2011) Rossby wave scales, propagation, and the variability of eddy-driven jets. *J Atmos Sci* 68(12):2893–2908. <https://doi.org/10.1175/JAS-D-11-039.1>
- Cattiaux J, Peings Y, Saint-Martin D et al (2016) Sinuosity of mid-latitude atmospheric flow in a warming world. *Geophys Res Lett* 43(15):8259–8268. <https://doi.org/10.1002/2016GL070309>
- Chan D, Zhang Y, Wu Q et al (2020) Quantifying the dynamics of the interannual variabilities of the wintertime East Asian Jet Core. *Clim Dyn* 54(3):2447–2463

- Chen G, Lu J, Burrows DA (2015) Local finite-amplitude wave activity as an objective diagnostic of midlatitude extreme weather. *Geophys Res Lett* 42:10952–10960. <https://doi.org/10.1002/2015GL066959>
- Chen G, Nie Y, Zhang Y (2022) Jet stream meandering in the northern hemisphere winter: an advection-diffusion perspective. *J Clim* 35(6):2055–2073. <https://doi.org/10.1175/JCLI-D-21-0411.1>
- Gao Z, Hu ZZ, Jha B et al (2014) Variability and predictability of Northeast China climate during 1948–2012. *Clim Dyn* 43(3):787–804
- Ghinassi P, Fragkoulidis G, Wirth V (2018) Local finite-amplitude wave activity as a diagnostic for Rossby Wave Packets. *Mon Weather Rev* 146(12):4099–4114. <https://doi.org/10.1175/MWR-D-18-0068.1>
- He J, Wu Z, Jiang Z et al (2006) Climate effect of Northeast cold vortex and its influence on MDeiyu. *Chin Sci Bull* 51(23):2803–2809
- Hersbach H, Bell B, Berrisford P et al (2020) The era5 global reanalysis. *Q J R Meteorol Soc* 146(730):1999–2049
- Holton JR (2004) An introduction to dynamic meteorology, Vol 88, 4th edn. Elsevier Academic Press. [https://doi.org/10.1016/S0074-6142\(04\)80036-6](https://doi.org/10.1016/S0074-6142(04)80036-6)
- Hoskins BJ, Karoly DJ (1981) The steady linear response of a spherical atmosphere to thermal and orographic forcing. *J Atmos Sci* 38(6):1179–1196. [https://doi.org/10.1175/1520-0469\(1981\)038<1179:TSLROA>2.0.CO;2](https://doi.org/10.1175/1520-0469(1981)038<1179:TSLROA>2.0.CO;2)
- Hu K, Lu R, Wang D (2010) Seasonal climatology of cut-off lows and associated precipitation patterns over northeast china. *Meteorol Atmos Phys* 106(1):37–48. <https://doi.org/10.1007/s00703-009-0049-0>
- Hu K, Lu R, Wang D (2011) Cold vortex over northeast china and its climate effect. *Chin J Atmos Sci (in Chinese)* 35(1):179–191
- Huang CS, Nakamura N (2015) Local finite-amplitude wave activity as a diagnostic of anomalous weather events. *J Atmos Sci* 73(1):211–229. <https://doi.org/10.1175/JAS-D-15-0194.1>
- Huang CS, Nakamura N (2017) Local wave activity budgets of the wintertime Northern Hemisphere: implication for the Pacific and Atlantic storm tracks. *Geophys Res Lett* 44(11):5673–5682. <https://doi.org/10.1002/2017GL073760>
- Lian Y, Boeh C, Xie Z et al (2010) The anomalous cold vortex activity in northeast china during the early summer and the low-frequency variability of the northern hemispheric atmospheric circulation. *Chin J Atmos Sci (in Chinese)* 32:429–439
- Lian Y, Shen B, Li S et al (2016) Mechanisms for the formation of northeast china cold vortex and its activities and impacts: an overview. *J Meteorol Res* 30:881–896
- Lin Z, Bueh C (2021) Formation of the northern East Asian low: role of diabatic heating. *Clim Dyn* 56(9):2839–2854
- Liu H, Wen M, He J et al (2012) Characteristics of the northeast cold vortex at intraseasonal time scale and its impact. *Chin J Atmos Sci (in Chinese)* 36:959–973
- Liu C, Liu Y, Liu X et al (2013) Dynamical and chemical features of a cutoff low over northeast China in July 2007: results from satellite measurements and reanalysis. *Adv Atmos Sci* 30(2):525–540
- Luo D, Chen X, Dai A et al (2018) Changes in atmospheric blocking circulations linked with winter Arctic warming: a new perspective. *J Clim* 31(18):7661–7678. <https://doi.org/10.1175/JCLI-D-18-0040.1>
- Luo D, Zhang W, Zhong L et al (2019) A nonlinear theory of atmospheric blocking: a potential vorticity gradient view. *J Atmos Sci* 76(8):2399–2427
- Martineau P, Chen G, Burrows DA (2017) Wave events: climatology, trends, and relationship to Northern Hemisphere winter blocking and weather extremes. *J Clim* 30(15):5675–5697. <https://doi.org/10.1175/JCLI-D-16-0692.1>
- Nakamura H (1994) Rotational evolution of potential vorticity associated with a strong blocking flow configuration over Europe. *Geophys Res Lett* 21(18):2003–2006
- Nakamura N, Huang CS (2018) Atmospheric blocking as a traffic jam in the jet stream. *Science* 361(6397):42–47. <https://doi.org/10.1126/science.aat0721>
- Nieto R, Gimeno L, de la Torre L et al (2005) Climatological features of cutoff low systems in the Northern Hemisphere. *J Clim* 18(16):3085–3103
- O'Reilly CH, Minobe S, Kuwano-Yoshida A (2016) The influence of the Gulf Stream on wintertime European blocking. *Clim Dyn* 47(5):1545–1567
- Palmén E, Newton C (1969) The mean structure of the atmosphere, and the maintenance of the general circulation in the Northern Hemisphere. In: Atmospheric circulation systems, international geophysics, vol 13. Academic Press, pp 1–25. [https://doi.org/10.1016/S0074-6142\(08\)62790-4](https://doi.org/10.1016/S0074-6142(08)62790-4)
- Saha S, Moorthi S, Wu X et al (2014) The ncep climate forecast system version 2. *J Clim* 27(6):2185–2208. <https://doi.org/10.1175/JCLI-D-12-00823.1>
- Screen JA, Simmonds I (2013) Exploring links between Arctic amplification and mid-latitude weather. *Geophys Res Lett* 40(5):959–964. <https://doi.org/10.1002/grl.50174>
- Seager R, Harnik N, Kushnir Y et al (2003) Mechanisms of hemispherically symmetric climate variability. *J Clim* 16:2960–2978
- Takaya K, Nakamura H (2001) A formulation of a phase-independent wave-activity flux for stationary and migratory quasigeostrophic eddies on a zonally varying basic flow. *J Atmos Sci* 58(6):608–627. [https://doi.org/10.1175/1520-0469\(2001\)058<0608:AFOAP I>2.0.CO;2](https://doi.org/10.1175/1520-0469(2001)058<0608:AFOAP I>2.0.CO;2)
- Tibaldi S, Molteni F (1990) On the operational predictability of blocking. *Tellus A* 42(3):343–365. <https://doi.org/10.1034/j.1600-0870.1990.t01-2-00003.x>
- Wang D, Zhong S, Liu Y et al (2007) Advances in the study of rainstorm in Northeast China. *Adv Earth Sci* 22(6):549–560
- Wang D, Chen H, Zhao C (2018) Connection between spring land surface thermal anomalies over west asia and decadal variation of early summer cold vortex in Northeast China. *Chin J Atmos Sci* 42:70–80
- Wang M, Zhang Y, Lu J (2021) The evolution dynamical processes of Ural blocking through the lens of local finite-amplitude wave activity budget analysis. *Geophys Res Lett*. <https://doi.org/10.1029/2020GL091727>
- Xie Z, Bueh C (2015) Different types of cold vortex circulations over Northeast China and their weather impacts. *Mon Weather Rev* 143(3):845–863. <https://doi.org/10.1175/MWR-D-14-00192.1>
- Yang B, Wang L, Guan Y (2021) Characteristics and development mechanisms of northeast cold vortices. *Adv Meteorol* 6636:192
- Zhao S, Sun J (2007) Study on cut-off low-pressure systems with floods over Northeast Asia. *Meteorol Atmos Phys* 96(1):159–180